Magnetic transitions and different valence states of manganese ions in solid solutions (Ni,Cu,Mn)$_3$BO$_5$

© S.N. Sofronova[1], E.V. Eremin[1], A.A. Veligzhanin[2], A.V. Chernyshov[1], A.V. Kartashev[2], D.A. Velikanov[1]

[1] Kirensky Institute of Physics Federal Research Center „Krasnoyarsk Scientific Center of the Siberian Branch of RAS",
Krasnoyarsk, Russia
[2] National Research Center, „Kurchatov Institute",
Moscow, Russia

E-mail: ssn@iph.krasn.ru

The content of metal ions and their valence state for three Ni$_x$Cu$_y$Mn$_{3-x-y}$BO$_5$ compositions were estimated by EXAFS and XANES spectroscopy methods. In all three compositions, the copper y content did not exceed 0.25; in the third composition, some manganese ions entered the compound not only in the trivalent, but also in the divalent state. A detailed study of the magnetic properties showed that two magnetic transitions are observed in all compositions: one in the region of $60-75$ K, and the second in the region of 10 K. Based on the exchange interactions calculated within the framework of the empirical model, the magnetic ordering temperatures for two- and three-lattice magnets were determined and it was assumed that the magnetic transition in the region of $60-75$ K is associated with the ordering of magnetic moments in positions 2 and 3.

Keywords: ludwigites, magnetic phase transition, indirect exchange interactions.

1. Introduction

Transition metal oxyborates, due to geometric features of their structure, can be classified as quasi-low-dimensional compounds [1–7]. In oxyborates with ludwigite structure two subsystem of metal ions are often distinguished: the first subsystem is formed by metal ions in positions 2 and 4, the second subsystem is formed by metal ions in positions 3 and 1 (Fig. 1). Exchange couplings inside subsystems are similar to such structural elements as „three-leg ladders" [2,3,8]. Exchange paths between subsystems form triangle groups, that in case of antiferromagnetic interactions results in a strong competition of exchange couplings and occurrence of frustrations. In Fe$_3$BO$_5$ [8] and Cu$_2$MnBO$_5$ [9] the magnetic system is split into two subsystems connected exactly with the three-leg ladders. In addition, magnetic moments of subsystems are oriented normally in Fe$_3$BO$_5$ and at an angle of about 60 degrees in Cu$_2$MnBO$_5$. (Ni,Mn)$_3$BO$_5$ ludwigites are not as well studied as Fe$_3$BO$_5$ and Cu$_2$MnBO$_5$ [10–12], however, these compounds are interesting due to the fact that manganese can be included in them in different valence states [11]. In particular, previously we have obtained compositions, where in addition to three-valence ions of manganese, four-valence ions of manganese were presented as well [11]; in addition, in the Mn$_{1.2}$Ni$_{1.8}$BO$_5$ ludwigite the magnetization reversal effect can be present [12]. Magnetization inversion and noncollinear magnetization are effects that are interesting from the fundamental point of view as well as in terms of technological applications.

The investigation of Ni$_2$MnBO$_5$-Cu$_2$MnBO$_5$ solid solutions is interesting because the parent compounds Ni$_2$MnBO$_5$ and Cu$_2$MnBO$_5$ have different crystal structure and magnetic properties.

In our previous study [13] we made an attempt to obtain a number of compounds of solid solutions of Ni$_2$MnBO$_5$-Cu$_2$MnBO$_5$ by substituting nickel ions with copper ions. However, it appeared that copper ions were presented in these compounds only in small amounts, even in the case when copper was the predominant element in the solution-melt system. In [13,14] we have presented a detailed
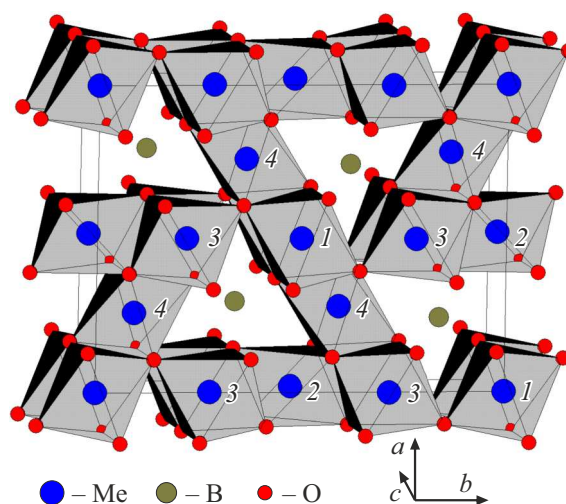

Figure 1. ludwigite structure.

description of the growth experiment and the investigation of magnetic properties of one of produced compounds. In this study we present a detailed investigation of structural properties by methods of Mössbauer spectroscopy EXAFS and transmission spectroscopy XANES, theoretical calculations that evaluate the probability of copper ions distribution over different crystallographic positions, and a detailed investigation of magnetic properties, as well as an evaluation of exchange couplings within an empirical model for all obtained compositions.

2. Experimental and theoretical studying

Previously we have obtained three compositions with considerably different initial charge contents of metal ions in them; however, investigations of compositions of the produced single-crystals by transmission microscope have shown that copper is included in the investigated compounds in minor quantities. This is indirectly confirmed by results of structural investigations by X-ray diffraction methods because all three compositions $(Ni, Cu, Mn)_3BO_5$ have rhombic space group. With a significant copper content monoclinic distortions would arise in the compounds due to the Jahn–Teller effect of copper ions, as in Cu_2MnBO_5.

The investigation of copper, manganese, and nickel absorption spectra by methods of EXAFS and XANES spectroscopy of $(Ni, Cu, Mn)_3BO_5$ for three different compositions allowed refining the content of metal ions, determining valence states, and studying the local environment of manganese and nickel ions. The measurement procedure is described in detail in our study [10].

Absorption spectra at the K-edge of copper and nickel for all three compositions are almost identical, the spike at the K-edge corresponds to divalent standards of CuO and NiO. Thus, a conclusion can be made that copper and nickel ions are included in the compounds under study in a divalence state. Fig. 2 shows EXAFS absorption spectra and the spike
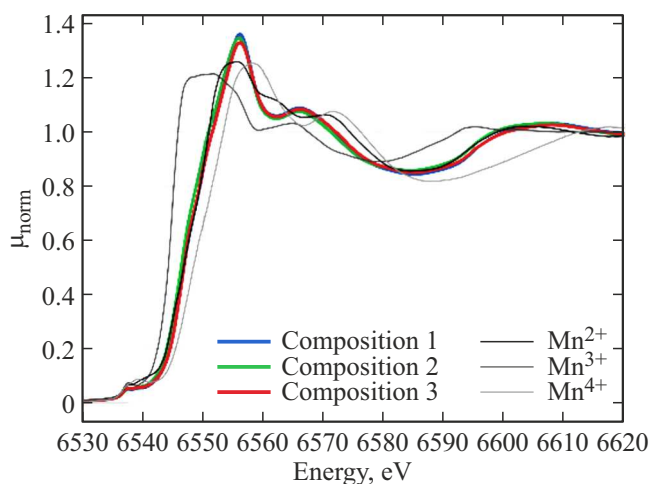

Figure 2. EXAFS absorption spectra and a spike at the K-edge of absorption for manganese ions.

Table 1. Contents of metal ions in investigated compounds. Coefficients are reduced to the content in the formula unit of ludwigite $Me_x^1 Me_y^2 Me_{3-x-y}^3 BO_5$

	Composition 1	Composition 2	Composition 3
EXAFS method			
Mn	1.04	1.06	1.22
Ni	1.85	1.73	1.57
Cu	0.11	0.21	0.21
EXAFS method			
Mn	0.97	0.94	1.12
Ni	1.87	1.78	1.59
Cu	0.16	0.28	0.29

Table 2. Structural model of the local environment near a nickel atom. Nickel–metal scattering paths are insensitive to the type of metal

Central atom	Scattering path	Coordination number N	Initial distance R, Å
Ni	Ni−O	6	2.0772
	Ni−B	4	3.0564
	Ni−Ni*	2	3.0329
	Ni−Ni*	4	3.0879

at K-edge of manganese ion absorption for investigated compositions and standards. It can be seen from the figure, that absorption spectra of manganese at the K-edge are slightly different for the compositions. In composition 3 the main growth at the K-edge shifts toward the standard for the manganese in divalence state.

Based in the magnitude of spike at the K-edge of absorption, compositions of compounds were recalculated, which are shown in Table. 1 in comparison with the results obtained by methods of transmission spectroscopy.

As can be seen from Table 1, the results obtained by different methods qualitatively match each other. The content of copper in compositions 2 and 3 is nearly the same, however the content of manganese is different. Part of manganese ions in composition 3, due to the condition of electroneutrality, must be in a divalence state, while in compositions 1 and 2 manganese ions are predominantly in a three-valence state.

For the investigation of local environment, position 1 (Fig. 1) was used as an initial approximation at the nickel edges, since it is more symmetric, however the approximation additionally excluded all paths with minor differences in R distances. In the final model we used paths listed in Table 2.

In the process of approximation changes in interatomic distances, Debye–Waller factors for each type of atoms were determined, as well as the shift of zero and the total amplitude of oscillations. Coordination numbers N were fixed. The hypothesis of oxygen coordination sphere splitting was
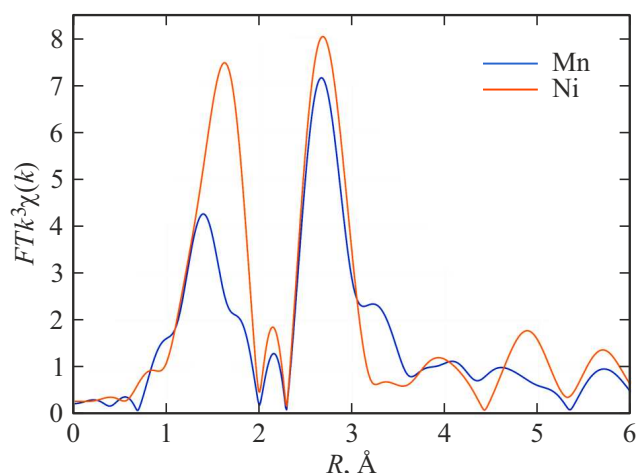
Figure 3. Comparison of the local environment of nickel and manganese in a compound with composition 1.

Table 3. Structural model of the local environment near a manganese atom. Nickel–metal scattering paths are insensitive to the type of metal

Central atom	Scattering path	Coordination number N	Initial distance R, Å
Mn	Mn−O	4	1.9664
	Mn−O	2	1.9664
	Mn−Ni	1	2.7768
	Mn−Mn	6	3.0018
	Mn−Ni	2	3.3358

verified, however it did not result in approximation quality improvement, and interatomic distances Ni−O in this case were determined in an unstable manner. The scattering path Ni−B was added to improve quality of the adjustment.

The local environment of manganese is considerably less symmetric. Fig. 3 shows comparison of the local environment for a compound with composition 1. It can be seen, that peak in the region of $1-2$ Å that corresponds to metal–oxygen distance, is considerably lower for manganese, which corresponds to a disordered coordination sphere with several non-equivalent manganese–oxygen distances.

When describing the manganese absorption edge, position 4 (Fig. 1) is used in the initial approximation, which is populated by three-valence ions in majority of ludwigites. At the same time, the description of local structure includes scattering paths listed in Table 2. To take into account the oxygen sphere splitting, two independent oxygen scattering paths were determined with coordination numbers 2 and 4, respectively. Alternative variants of splitting do not yield approximation quality improvement or do not yield stable approximating parameters for the local structure. As in the case of nickel local environment, interatomic distances, Debye–Waller factors for each type of atoms were determined, as well as the shift of zero and the total amplitude of oscillations. Coordination numbers were fixed. The obtained structural parameters, as well as approximation ranges in the k- and R-space are shown in Tables 3 and 4.

As a result of the approximation it is found, that the manganese local environment is characterized by four short distances Mn−O1 ($R \sim 1.99$ Å) and two long distances Mn−O2 ($R \sim 2.2$ Å). Composition 3 with the highest content of manganese is characterized by a longer distance Mn−O1 ($R \sim 2.0$ Å) and a higher Debye–Waller factor, which is indicative of more disordered oxygen environment, that can be interpreted as the population by manganese

atoms of a larger number of various atomic positions in the structure as compared with other samples.

Parameters obtained for the local environment of nickel for three investigated samples coincide with each other within the limits of error. The length of path Ni−B is significantly different from that of the crystal model ($R \sim 2.8$ Å as opposed to $R \sim 3.05$ Å according to the data of X-ray diffraction), which, along with the low Debye–Waller factor for this path ($\sigma^2 \sim 1-2 \cdot 10^{-3}$ Å^2), low sensitivity of the method to this type of atoms due to low atomic number Z, allows suggesting that this path has no physical meaning and compensates for break effects in EXAFS spectra.

By analyzing the local environment of ions obtained by XANES method and the information on lengths of the Me−O bond obtained by the method of X-ray diffraction, a conclusion can be made that positions 1 and 3 are predominantly occupied by ions of nickel in all three compositions. In the Cu_2MnBO_5 compound the oxygen octahedra around copper ions are much more elongated, than the oxygen octahedra around manganese ions. Manganese ions in a divalence state have electron configuration d^5, and arising of the Jahn–Teller effect is not typical for them, as opposed to the three-valence manganese. In composition 3 the octahedron around the ion in position 4, according to X-ray diffraction data, is less elongated than that in compositions 1 and 2. This can be an indirect indication of the fact that the divalence manganese in composition 3 prefers to occupy position 4. The oxygen octahedra around ions in position 3 are distorted as well, but they are compressed, not elongated. Elongated octahedron is typical for the oxygen environment of manganese ions, and especially copper ions; our supposal is that position 3 is also predominantly occupied by nickel ions in all three compositions.

Since it is difficult to determine by X-ray diffraction and XANES spectroscopy methods the position, which is predominantly occupied by copper ions, we calculated energies of different cation ordered states within ab initio approach using Wien2K software package. A lattice cell contains twelve metal ions. Due to the condition of electroneutrality, four metal ions must be three-valence ions (we suppose that these are manganese ions) and eight ions

Table 4. Structural parameters for the local environment of manganese and nickel atoms obtained from X-ray absorption spectra

Sample	R_f, %	Adjustment range	S_0^2	E_0	Path	N	R, Å	σ^2, 10^{-3} Å^2
Mn (composition 1)	2.37	k: 2.0−11.0 R: 1.0−3.4	0.67 ± 0.14	5.6 ± 1.5	Mn−O1	4	1.993 ± 0.024	8.4 ± 4.8
					Mn−O2	2	2.203 ± 0.063	8.4 ± 4.8
					Mn−Ni1*	1	2.874 ± 0.073	4.2 ± 2.3
					Mn−Ni2*	6	3.092 ± 0.019	4.2 ± 2.3
					Mn−Ni3*	2	3.315 ± 0.035	4.2 ± 2.3
Mn (composition 2)	2.54	k: 2.0−11.0 R: 1.0−3.4	0.63 ± 0.13	5.5 ± 1.5	Mn−O1	4	1.988 ± 0.024	7.8 ± 4.4
					Mn−O2	2	2.204 ± 0.062	7.8 ± 4.4
					Mn−Ni1*	1	2.886 ± 0.076	4.3 ± 2.3
					Mn−Ni2*	6	3.094 ± 0.020	4.3 ± 2.3
					Mn−Ni3*	2	3.321 ± 0.037	4.3 ± 2.3
Mn (composition 3)	3.26	k: 2.0−11.0 R: 1.0−3.4	0.65 ± 0.15	5.7 ± 1.8	Mn−O1	4	2.022 ± 0.027	11.5 ± 7.2
					Mn−O2	2	2.221 ± 0.088	11.5 ± 7.2
					Mn−Ni1*	1	2.895 ± 0.087	4.2 ± 2.6
					Mn−Ni2*	6	3.106 ± 0.026	4.2 ± 2.6
					Mn−Ni3*	2	3.316 ± 0.047	4.2 ± 2.6
Ni (composition 1)	0.34	k: 2.0−11.0 R: 1.1−3.2	0.91 ± 0.10	−1.0 ± 1.0	Ni−O	6	2.062 ± 0.007	9.0 ± 1.3
					Ni−B	4	2.800 ± 0.039	1.8 ± 1.7
					Mn−Ni1*	2	2.922 ± 0.030	3.2 ± 1.1
					Mn−Ni2*	4	3.067 ± 0.011	3.2 ± 1.1
Ni (composition 2)	0.43	k: 2.0−11.0 R: 1.1−3.2	0.83 ± 0.10	−0.7 ± 1.2	Ni−O	6	2.060 ± 0.007	8.1 ± 1.4
					Ni−B	4	2.800 ± 0.044	1.1 ± 1.7
					Mn−Ni1*	2	2.927 ± 0.039	3.0 ± 1.5
					Mn−Ni2*	4	3.068 ± 0.013	3.0 ± 1.5
Ni (composition 3)	0.42	k: 2.0−11.0 R: 1.1−3.2	0.90 ± 0.09	−0.7 ± 1.1	Ni−O	6	2.064 ± 0.007	8.4 ± 1.3
					Ni−O	6	2.064 ± 0.007	8.4 ± 1.3
					Mn−Ni1*	2	2.939 ± 0.041	3.8 ± 1.7
					Mn−Ni2*	4	3.075 ± 0.011	3.8 ± 1.7

Here R_f — R-factor; S_0^2 — signal amplitude attenuation factor; E_0 — energy shift of photoelectron pulse origin in relation to the position of K-edge of absorption; N — coordination numbers of the closest neighbors in relation to the central atom; σ^2 — root-mean-square change in the bond length for atom pairs that takes into account thermal oscillations and static disordering of the local environment.

must be double-valence ions (nickel ions and copper ions substituting them). The calculation was performed for two concentrations: in the first case one ion of nickel was substituted by copper, in the second case two nickel ions were substituted by copper. Manganese ions occupied position 4 (Fig. 1), while copper ions we placed in the remaining three crystallographic positions and calculated the total energy of the crystal. The calculation was performed for a non-magnetic state and a ferromagnetic state.

The electronic structure was calculated using the method of FP-LAPW+LO [15,16]. The exchange-correlation energy was calculated using LSDA [17] and GGA-PBE [18] with additional Hubbard correlation coefficients that describe the local electron-electron repulsion related to $3d$-bands of Ni (LSDA+U and GGA-PBE+U) [19,20]. In our calculations we used experimental parameters of lattice and atom coordinates of compositions with concentrations of copper ions close to 0.125 and 0.25. The $R_{MT} \cdot K_{max}$ value in the calculations was pre-defined as 7.0. The energy in self-consistent calculations converged to $1\,\mu$Ry. The total energy was minimized with the use of set of 400 k-points in the

full Brillouin zone of the lattice cell. Radii of MT-spheres were 1.96 atomic units for Ni, 1.89 atomic units for Cu, 1.98 atomic units for Mn, 1.20 atomic units for B, and 1.39 atomic units for O. The total density of states (DoS) was calculated using the modified tetrahedron method of Blechl et al. [21]. In LSDA+U and GGA-PBE+U schemes we used parameters $U = 0.52\,$Ry for Cu and Ni ions, $U = 2.52\,$Ry for Mn and $J = 0\,$Ry.

Based on the calculation results, both compositions are found to be dielectric with a gap width of about 4 eV. Table 5 shows the difference of energies between the total energies in the case of copper ions located in different crystallographic lattices and the total energy in the case of position 2 populated by copper ions.

The table presents examples of population with the lowest energy, but not all possible variants for a concentration of 0.25.

As can be seen from Table 5, copper prefers to substitute nickel in position 2. Magnetic moments of nickel, copper, and manganese ions for the calculation of ferromagnetic structure are 1.78, 0.81 and 3.85 μ_B, respectively, which
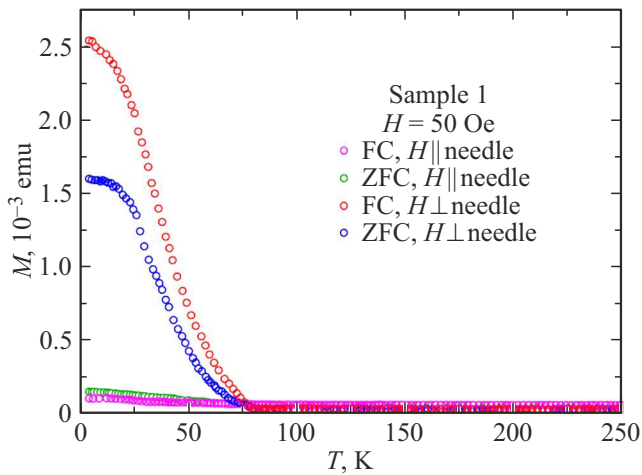
Figure 4. Dependence of magnetization versus temperature for single-crystal samples with composition 1.

match well the nominal values for two-valence ions of copper and nickel, as well as three-valence manganese ion.

Magnetic properties of compounds were studied at a PPMS Quantum design setup and a SQUID-magnetometer in the temperature range of $4-300$ K and the magnetic field strength range of $-90-90$ kOe. Detailed information on composition 2 is given in our previous study [14]. In this study we present a detailed investigation of compositions 1 and 3. Single crystal samples of all compositions were similar to needles, detailed description and photos of samples are shown in [13]. Crystallographic direction that corresponds to the direction along the needle is the c axis (corresponds to the lowest parameter of the lattice). It was not possible to orient the needles along two other directions (axes a and b) due to the small lateral sizes of samples.

Table 5. Difference of the total energies in the case when copper ions are located in different crystallographic positions and the total energy in the case of position 2 populated by copper ions

	Position of copper ions	ΔE
0.125		
	1 (2a)	0.0081
	2 (2d)	0
	3 (4g)	0.0112
	4 (4h*) (Mn$-$2d)	0.0452
0.25		
	3 (4g)	0.0224
	1 (2a)	0.0156
	2 (2d)	0
	1 and 2 (2a, 2d)**	0.0081
	1 and 2 (2a, 2d)***	0.0093

N o t e . * In the case of copper ions populating position 4, manganese ions from position 4 occupied position 2. ** Coordinates of copper ions: $(0, 0, 0)$ and $(0, 1/2, 1/2)$. *** Coordinates of copper ions: 1 $(0, 0, 0)$ and $(1/2, 0, 1/2)$.

Temperature dependencies of magnetization of the single crystal sample for composition 1 were measured with a magnetic field applied along and across the needle on a SQUID-magnetometer in a field of 50 Oe (Fig. 4), as well as on a PPMS unit for different fields. However, due to the small size of the sample and its low mass, measurements obtained at a PPMS unit have a very high level of noise and in this work we have only reported field dependencies of magnetization.

As can be seen from Fig. 4, when the magnetic field is applied along the needle, the magnetization growth is quire weak. When the magnetic field is applied across the needle, a growth of magnetization is observed below 75 K. Magnetizations measured in field-cooled and zero-field-cooled modes are different throughout the entire range of temperatures below the magnetic transition. The dependencies of magnetization versus field for the single crystal sample of composition 1 were measured at a PPMS setup and shown in Fig. 5. Hysteresis loops are
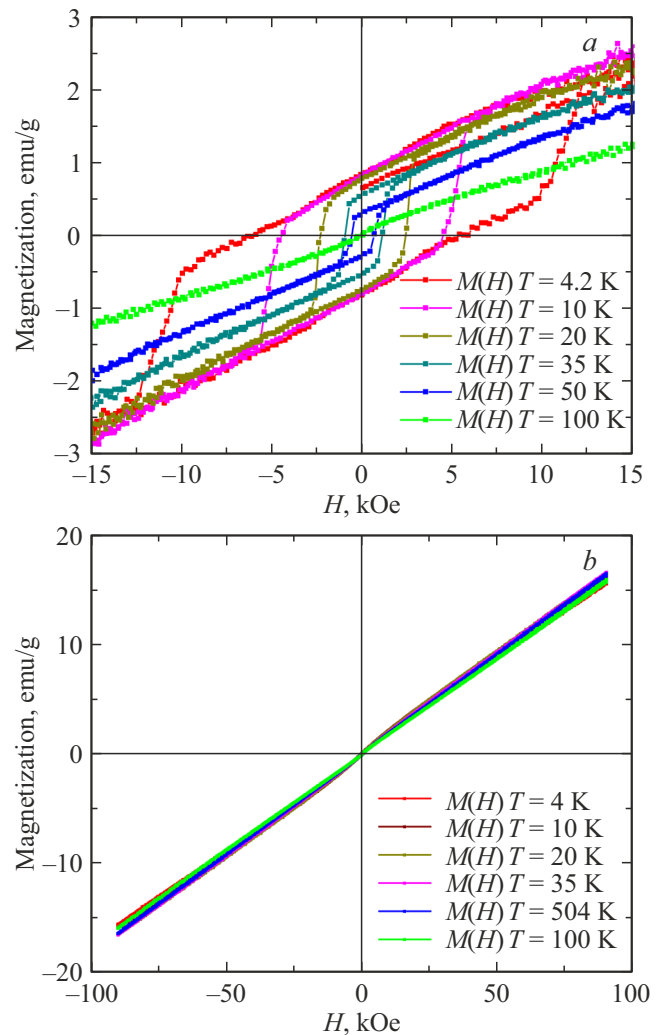

Figure 5. Dependencies of magnetization versus field for a single-crystal sample with composition 1 when the field is applied across (a) and along (b) the needle.

observed on the dependencies of magnetization versus field when the magnetic field is oriented across the needle. It should be noted, that the shape of hysteresis loops with temperature decrease is remained, the coercive field grows with temperature decrease. When a magnetic field is applied along the needle, the magnetization slightly deviates from the linear law at high temperatures and keeps a nearly unchanged slope.

Temperature and field dependencies of magnetization for composition 3 are shown in Fig. 6 and 7. It can be seen from the figures: as with composition 1, when a magnetic field is applied across the needle, hysteretic loops and a significant magnetization growth are observed, however, the transition temperature decreases down to 67 K, while with a field applied along the needle the magnetization growth is monotonous without distinct features. In the case of measurements in the zero-field-cooled mode, due to the residual field the magnetization at low temperatures is negative, a field of 1 kOe is insufficient to reorient magnetic moments immediately along the field and the reorientation takes place at a temperature near 20 K. When a magnetic field is applied along the needle at low temperatures, the magnetization in the zero-field-cooled (ZFC) and field-cooled (FC) modes is different. Field dependencies of the magnetization with a field applied across the needle in the temperature range of 10−50 K have a shape similar to those dependencies for composition 1. However, at 4 K the shape of hysteresis loop is slightly changed. Probably one more sublattice becomes ordered below 10 K. When a field is applied along the needle, field dependencies of magnetization, in contrast to composition 1, are considerably different from linear dependencies below the temperature of magnetic transition.

In compositions 1 and 2, manganese ions are mainly in a three-valence state, and despite the two times difference in copper concentration (0.11 and 0.21, respectively), the growth of magnetization starts in the region of 75 K. In composition 3 part of the copper is in a two-valence state, and the start temperature of magnetic ordering decreases. It should be noted, that in all compositions the magnetization is not zero until room temperatures. The content of copper in the solid solution has an effect on the coercive field, which grows with increase in copper content. In compositions 2 and 3, where copper content is nearly the same, the coercive field also is almost the same (about 18 kOe), while in composition 1 the coercive field is almost two times lower. Regardless the fact that magnetic moment of copper is lower that of manganese and nickel, with increase in copper content the magnetization grows. Probably, the magnetic subsystem, which is ordered in the region of 70 K, is ferromagnetic and includes, for example, positions 2 (nickel) and 4 (manganese), which are oriented antiparallel; in this case a decrease in magnetic moment in position 2 will result in an increase in the sum magnetization.

Dependencies of ac-susceptibility magnetization versus temperature for polycrystalline samples with compositions 1
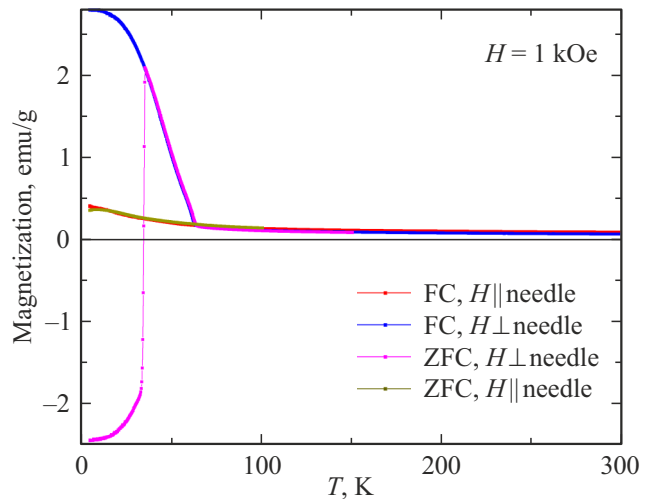

Figure 6. The dependencies of magnetization versus temperature for a sample with composition 3 when a magnetic field of 1 kOe is applied along and across the needle recorded in the zero-field-cooled (ZFC) and field-cooled (FC) modes.
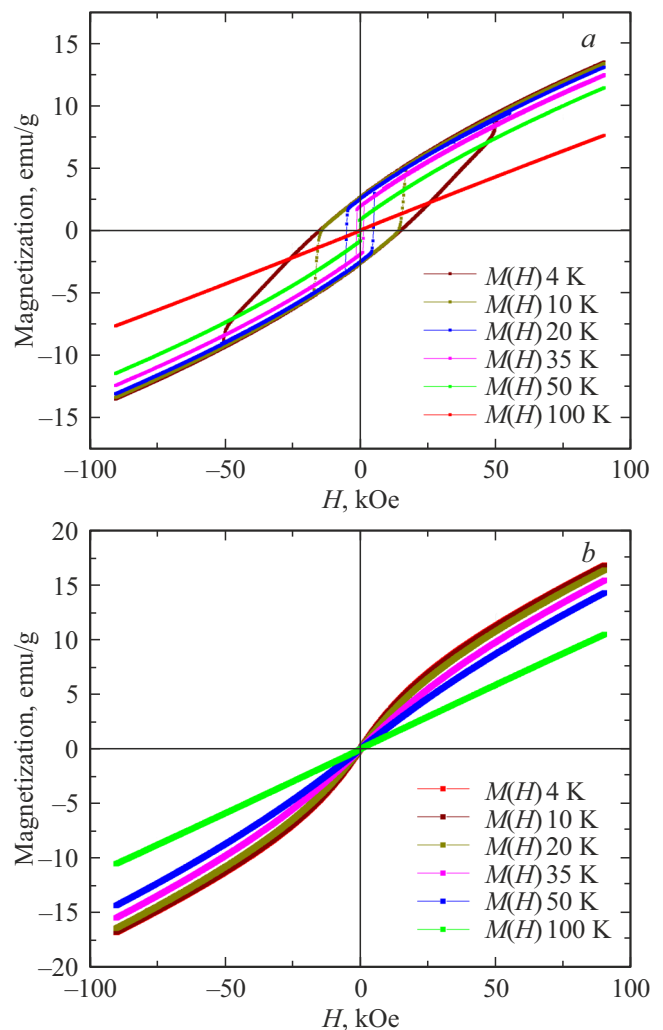

Figure 7. Dependencies of magnetization versus field for a single-crystal sample with composition 1 when the field is applied across (*a*) and along (*b*) the needle.
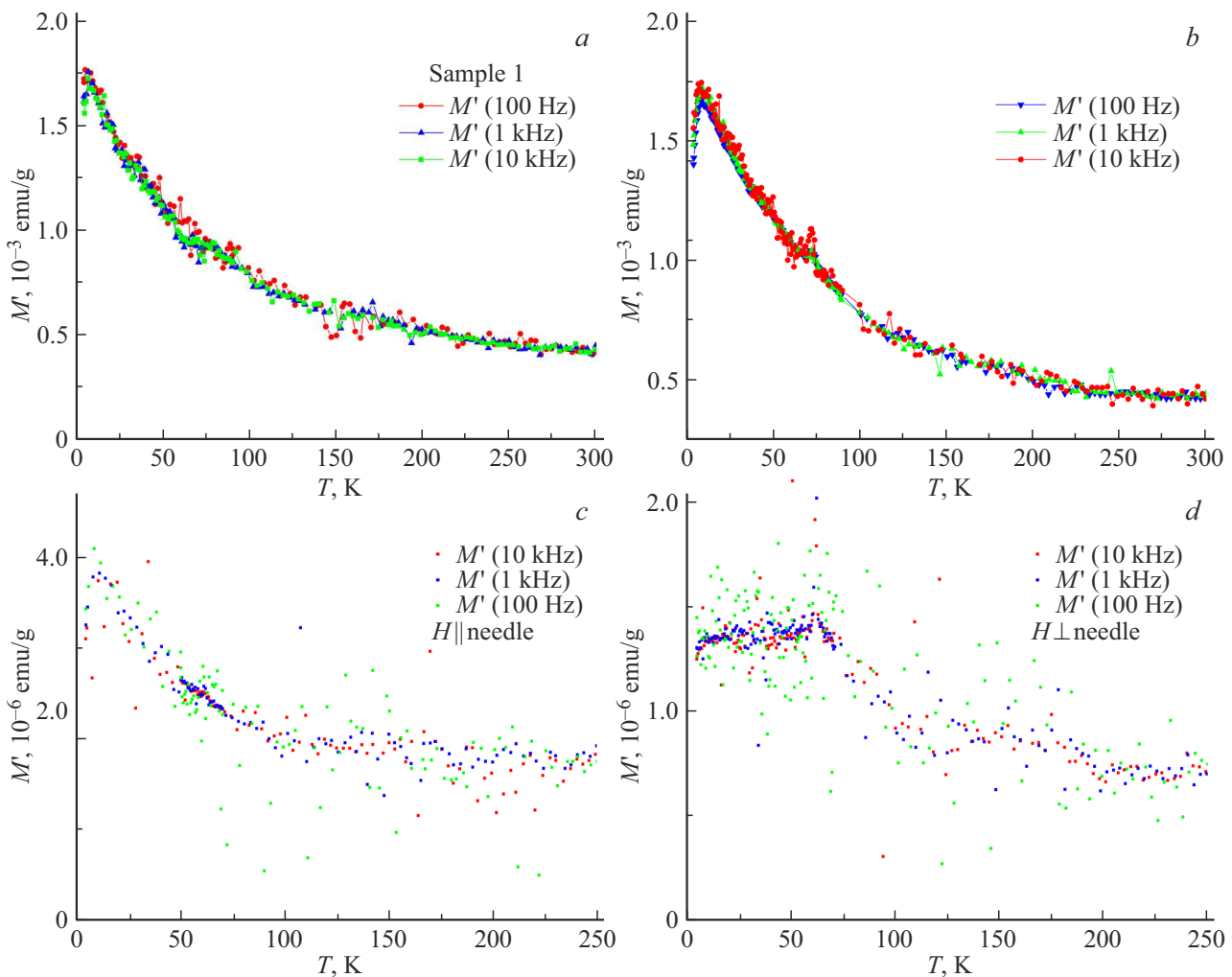
Figure 8. Temperature dependence of AC-susceptibility of polycrystal samples of compositions 1 and 2, single crystal sample of composition 3 with an alternating field applied along and across the needle.

and 2 shown in Fig. 8, *a* and *b* demonstrate smooth growth with temperature decrease from the room temperature. In the region of 75 K there is a feature: a small peak or a plateau; in this temperature range a magnetization growth is observed on the DC-magnetization when a field is applied across the needle. In the region of 10 K a sharp peak is observed in compositions 1 and 2. For composition 3 measurements of AC-susceptibility were carried out on a single crystal sample with a field applied along and across the needle (Fig. 8, *c* and *d*). With a field applied across the needle, an intensive growth of the AC-susceptibility starts below 100 K, in the region of 60 K a small peak is observed, then the dependence has a plateau until low temperatures. With a magnetic field applied along the needle, a peak near 10 K is observed. Thus, an assumption can be made that in all compounds there are two features: in the region of 65−75 K and below 15 K. In the range of 65−75 K part of magnetic moments is ordered in the direction normal to the needle, and below 15 K magnetic moments are ordered along the needle. Since the magnetization along the needle

grows weakly, the magnetic subsystem that ordered at low temperatures is an antiferromagnetic subsystem.

To analyze the magnetic behavior, we have plotted the $d\chi T/dT$ dependence for compositions 1 and 3, which is proportional to heat capacity. As can be seen from Fig. 9, there are two features on the curve: at low temperatures (10−15 K) and in the region of 50−60 K. For composition 3 we have also investigated heat capacity using the same method as in [14]. The excess heat capacity is shown in Fig. 10, where the dependence of $d\chi/dT$ is represented as well. As can be seen from Fig. 8, 9, and 10, features on temperature dependencies of $d\chi T/dT$, AC-susceptibility, and heat capacity match each other. Values of $d\chi T/dT$ in the range of 30−100 K are negative, and below 30 K they are positive. According to [22], for antiferromagnetics the $d\chi T/dT$ derivative in the region of Neel temperature T_N is positive; in our case, probably, the low-temperature transition is related to the antiferromagnetic ordering; then the transition in the region of 50−60 K the most likely is a ferromagnetic ordering,
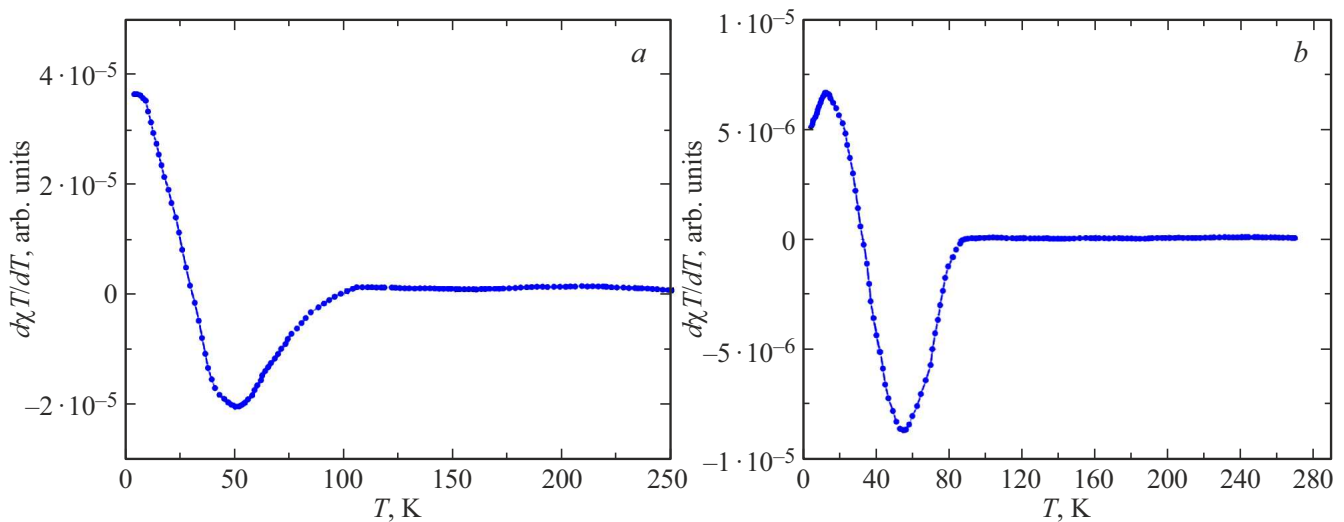
Figure 9. Temperature dependence of $d\chi T/dT$ for compositions 1 (*a*) and 3 (*b*).

which matches both the temperature and field dependencies of magnetization.

In [10,11,14] we evaluated indirect exchange couplings in the Ni_2MnBO_5 compound. In this study we have evaluated how indirect exchange couplings change for all three compositions assun=ming that ions of copper occupy position 2, as it follows from the ab initio calculation. When calculating indirect exchange couplings for composition 3, we also assumed that ions of the two-valence manganese occupy position 2, although within the ab initio calculation no such investigations were carried out, since due to the aliovalent state of manganese ions we have faced problems with the calculation convergence.

Table 6 shows indirect exchange couplings related to position 2, which are calculated for different compositions; other exchange couplings remain unchanged.

It can be seen from the table, that ninety-degree exchanges 2−2 and 2−4 remain ferromagnetic and antiferromagnetic, although the exchange magnitude changes. The 165-degree exchange coupling 2−4 in the case of replacement with copper becomes antiferromagnetic. The exchange coupling 2−3 in compositions 1 and 2 changes a little, while in composition 3 it becomes significantly weaker.

The behavior of heat capacity and AC-susceptibility shows that there are two features: in the region of 60−75 K and at low temperatures of 10−40 K. Probably, a part of magnetic moments becomes ordered in the region of 60−75 K (depending on composition), in this case magnetic moments become oriented normal to the needle; then with decrease in temperature other magnetic moments start to order, however these magnetic moments are oriented along the needle. As we noted before, in the ludwigite structure exchange paths form two three-leg ladders (4−2−4 and 3−1−3), between which triangle groups are formed. The magnetic system in many ludwigites
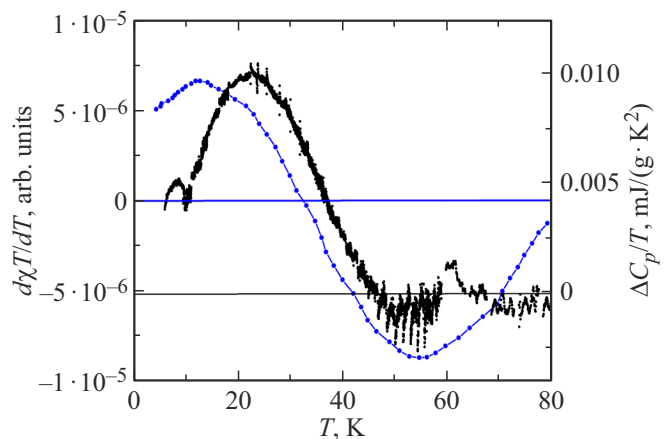

Figure 10. Temperature dependencies $d\chi T/dT$ and $\Delta C_p/T$ for composition 3.

is split into two subsystems related to three-leg ladders; in particular, in Cu_2MnBO_5 and Fe_3BO_5 magnetic moments of subsystems are noncollinearly oriented. In the Ni_2MnBO_5 ludwigite there are many competing exchange couplings. Chains of nickel ions along the short axis in positions 1, 2, and 3 are bound by ferromagnetic couplings, while manganese ions in position 4 are bound by antiferromagnetic coupling. As a result, in subsystem 4−2−4 there are many competing couplings. Ions in positions 2 and 3 are bound to each other by ferromagnetic couplings as well, and bound with ions in position 1 by antiferromagnetic couplings. There are no competing exchange couplings between ions in positions 1, 2, and 3. In the case of nickel replacement by copper and two-valence manganese, magnitudes of exchanges between ions in positions 1, 2, and 3 change, but the nature of exchange couplings remains unchanged. It can be assumed that in the region of 60−75 K (depending on

Table 6. Indirect exchange couplings (J) related to position 2d, which are calculated for different compositions

	J (Ni_2MnBO_5), K	J (Composition 1), K	J (Composition 2), K	J (Composition 3), K
2d−2d	6.7	7.9	10.0	6.6
2d−4h (90)	−4.6	−4.1	−3.1	−4.9
2d−4h (165)	1.1	−1.6	−2.6	−1.4
2d−4g	5.7	5.9	6.3	1.9

Table 7. Evaluation of magnetic ordering temperatures for two- and three-sublattice magnetic material for different variants of magnetic subsystems

Positions of ions, we relate magnetic subsystems with	Composition 1	Composition 2	Composition 3
1, 3	$T_{C1} = 31$ K, $T_{C2} = 14$ K	$T_{C1} = 31$ K, $T_{C2} = 14$ K	$T_{C1} = 31$ K, $T_{C2} = 14$ K
2, 3	$T_{C1} = 53$ K, $T_{C2} = $ neg*	$T_{C1} = 53$ K, $T_{C2} = $ neg*	$T_{C1} = 42$ K, $T_{C2} = 16$ K
1, 2, 3	$T_{C1} = 53$ K, $T_{C2} = 16$ K, $T_{C3} = $ neg*	$T_{C1} = 53$ K, $T_{C2} = 14$ K, $T_{C3} = $ neg*	$T_{C1} = 41$ K, $T_{C2} = 21$ K, $T_{C3} = 11$ K

N o t e . * Solving the equation results in a negative value, that has no physical meaning for the absolute temperature.

on composition) an ordering of magnetic moments in positions 1, 2, and 3 occurs. Using the calculated exchange couplings, we have evaluated the Curie temperature TC for two- and three- sublattice magnetic material. The evaluation results are given in Table 7.

As can be seen from Table 7, for compositions 1 and 2 the T_{C1} for sublattices 1−2−3 and 2−3 is the same, while for composition 3 it is lower, which matches the experimental results, if we assume that the magnetic transition in the region of 60−75 K is related to subsystem 2−3. Probably, in the region of 60−75 K magnetic moments in positions 1, 2, 3 (2, 3) are ordered, and at low temperatures ordering in position 4 takes place, however due to competing couplings, the ordering may be incomplete.

3. Conclusion

The investigation of three different compositions of $Ni_xCu_yMn_{3-x-y}BO_5$ by EXAFS and XANES spectroscopy allowed evaluating the content of metal ions and their valence state. The obtained information on the content of metal ions qualitatively matches the data obtained by the method of transmission spectroscopy. In all three compositions the content of copper was not greater than $y < 0.25$. Ions of nickel and copper are included in the composition of compounds in a two-valence state, manganese ions are included mainly in a three-valence state; however, in the third composition a part of manganese ions is included in the compound not only in a three-valence state, but also in a two-valence state. Calculations of total energies of different cation-ordered structures for two concentrations of copper ions $y = 0.125$ and $y = 0.25$ using Wien2K software package have shown that in both cases copper ions prefer to occupy position 2 (2d).

The detailed study of magnetic properties has shown that in all compositions two magnetic transitions are observed. The first transition is related to the ferromagnetic ordering of magnetic moments of part of ions normal to the short axis of the crystal in the region of 60−75 K, and the second transition in the region of 10 K is related to the antiferromagnetic ordering of magnetic moments along the short axis of the crystal. Based on the exchange couplings calculated within the empirical model, temperatures of magnetic ordering were evaluated for two- and three-sublattice magnetic material and a supposal is made that the magnetic transition in the region of 60−75 K is related to the ordering of magnetic moments in positions 1, 2, and 3; at low temperatures the antiferromagnetic ordering of magnetic moments in position 4 is possible.

Conflict of interest

The authors declare that they have no conflict of interest.

References

[1] L.N. Bezmaternykh, S.N. Sofronova, N.V. Volkov, E.V. Eremin, O.A. Bayukov, I.I. Nazarenko, D.A. Velikanov. Physica Status Solidi B **249**, *8*, 1628 (2012).

[2] E. Bertaut. Acta Crystallographica **3**, *6*, 473 (1950).

[3] H. Neuendorf, W. Gunser. J. Magn. Magn. Mater. **173**, *1−2*, 117 (1997).

[4] J.C. Fernandes, R.B. Guimarães, M.A. Continentino, H.A. Borges, J.V. Valarelli, A. Lacerda. Phys. Rev. B **50**, *22*, 16754 (1994).

[5] A. Arauzo, N.V. Kazak, N.B. Ivanova, M.S. Platunov, Y.V. Knyazev, O.A. Bayukov, L.N. Bezmaternykh, I.S. Lyubutin, K.V. Frolov, S.G. Ovchinnikov, J. Bartolomé. J. Magn. Magn. Mater. **392**, 114 (2015).

[6] A.M. Kadomtseva, Yu.F. Popov, G.P. Vorob'ev, A.P. Pyatakov, S.S. Krotov, K.I. Kamilov, V.Yu. Ivanov, A.A. Mukhin, A.K. Zvezdin, A.M. Kuz'menko, L.N. Bezmaternykh, I.A. Gudim, V.L. Temerov. Low Temp. Phys. **36**, *6*, 511 (2010).

[7] S.N. Sofronova, N.V. Kazak, E.V. Eremin, E.M. Moshkina, A.V. Chernyshov, A.F. Bovina. J. Alloys. Compounds **864**, 158200 (2021).

[8] P. Bordet, E. Suard. Phys. Rev. B **79**, *14*, 144408 (2009).

[9] E. Moshkina, C. Ritter, E. Eremin, S. Sofronova, A. Kartashev, A. Dubrovskiy, L. Bezmaternykh. J. Phys. Condens. Matter **29**, *24*, 245801 (2017).

[10] S. Sofronova, E. Moshkina, I. Nazarenko, A. Veligzhanin, M. Molokeev, E. Eremin, L. Bezmaternykh. J. Magn. Magn. Mater. **465**, 201 (2018).

[11] L.N. Bezmaternykh, E.M. Kolesnikova, E.V. Eremin, S.N. Sofronova, N.V. Volkov, M.S. Molokeev. J. Magn. Magn. Mater. **364**, 55 (2014).

[12] E. Moshkina, S. Sofronova, A. Veligzhanin, M. Molokeev, I. Nazarenko, E. Eremin, L. Bezmaternykh. J. Magn. Magn. Mater. **402**, 69 (2016).

[13] E. Moshkina, A. Bovina, M. Molokeev, A. Krylov, A. Shabanov, A. Chernyshov, S. Sofronova. Cryst. Eng. Commun. **23**, 5624 (2021).

[14] A. Kartashev, E. Eremin, E. Moshkina, M. Molokeev, S. Sofronova. J. Magn. Magn. Mater. **545**, 168747 (2022).

[15] P. Blaha, K. Schwarz, G. Madsen, D. Kvasnicka, J. Luitz. An Augmented Plane Wave + Local Orbitals Program for Calculating Crystal Properties. Vienna University of Technology, Inst. Phys. Theor. Chem., Vienna (2015).

[16] E. Sjöstedt, L. Nordström, D.J. Singh. Solid State Commun. **114**, *1*, 15 (2000).

[17] J.P. Perdew, Y. Wang. Phys. Rev. B **45**, *23*, 13244 (1992).

[18] J.P. Perdew, K. Burke, M. Ernzerhof. Phys. Rev. Lett. **77**, *18*, 3865 (1996).

[19] V.I. Anisimov, J. Zaanen, O.K. Andersen. Phys. Rev. B **44**, *3*, 943 (1991).

[20] V.I. Anisimov, I.V. Solovyev, M.A. Korotin, M.T. Czyyk, G.A. Sawatzky. Phys. Rev. B **48**, *23*, 16929 (1993).

[21] P.E. Blöchl, O. Jepsen, O.K. Andersen. Phys. Rev. B **49**, *23*, 16223 (1994).

[22] M.E. Fisher. Phil. Mag. **7**, **82**, 1731 (1962).